# Impact behavior of honeycombs under combined shear-compression, Part analysis

Bing Hou, Stephane Pattofatto, Yl Li, Han Zhao

HAL Id: hal-00580834
https://hal.science/hal-00580834

Submitted on 29 Mar 2011

# Impact behavior of honeycombs under combined shear-compression, PartⅡ analysis

B. HOU[1,2], S. PATTOFATTO[2], Y.L. LI[1], H. ZHAO[2,*]

[1]School of Aeronautics, Northwestern Polytechnical University, 710072 Xi'an, China

[2]Laboratoire de Mecanique et Technologie, ENS Cachan/CNRS UMR8535/UPMC Parisuniversitas/PRES UniverSud, 61 Avenue du président Wilson, 94235 Cachan Cedex, France

## Abstract

In this paper, a numerical virtual model of honeycomb specimen as a small structure is used to simulate its combined shear-compression behavior under impact loading. With Abaqus explicit code, response of such a structure made of shell elements is calculated under the prescribed velocities as those measured in the combined shear-compression test presented in the part I of this study.

The simulated results agree well with the experimental ones in terms of overall pressure/crush curves and deformation mode. It allows for the determination of the separated normal behavior and shear behavior of honeycomb specimen under dynamic combined shear-compression. It is found that the normal strength of honeycomb decreases with the increasing shearing load. Quasi-static calculations were also performed and a significant dynamic enhancement found in experiments was validated again in the numerical work. In the end, a crushing envelope of normal strength vs. shear strength plane was obtained on the basis of these simulations.

**Keywords:** honeycombs, combined shear-compression, FEM, dynamic enhancement.

# 1. Introduction

Dynamic multiaxial behavior of honeycombs as a basic energy-absorption design parameter is eagerly desired in order to perform numerical simulations for various industrial applications. Many previous works on this domain have been reported in the open literature and a large number of these works concern mainly the in-plane behavior, and mostly under quasi-static loading [1-5]. However, the most interesting behavior of honeycombs for an energy absorption application is the out-of-plane crushing behavior, especially the one under combined out-of-plane shear-compression which is the most realistic loading mode for such use.

Under quasi-static loading, some testing methods for the combined shear-compression loading have been reported [6-8] and were used to determine the yield envelope of aluminum honeycomb under this prescribed biaxial loading states [8-10]. For example, Hong et al. [8] derived a quadratic yield criterion suitable for orthotropic material by modifying Hill's quadratic yield criterion. Mohr et al. [9,10] suggested a linear fit for the crushing envelope based on their quasi-static calculated results.

Under dynamic loading, many reported works revealed that the strength of honeycomb under uniaxial dynamic compression is higher than under quasi-static loading [11-14], even if the shock wave effect is not involved [15]. However, the behavior of honeycombs under dynamic multiaxial loading is rarely reported up to now. The main reason for such situations lies in the difficulties to achieve dynamic multiaxial experiments with accurate data measurements.

Some previous works proposed the dynamic multiaxial testing methods using drop-weight or high speed machine [16,17], but the accuracy is not optimal at higher loading rate. In order to improve the measurement accuracy, we proposed in the Part I of this paper a new testing method using large diameter Hopkinson bars with beveled ends to perform combined shear-compression test under impact loading. It permits to obtain interesting overall force/crush curves but cannot give a separate normal and pure shear behavior. Thus, with the test presented in Part I, there is no mean to identify directly a given yield criterion.

In this part II of the work, a numerical approach is presented to study a yield criterion.

The dynamic and quasi-static combined shear-compression experiments are numerically reproduced with a detailed FEM model for the honeycomb specimen. The accuracy of these simulations is validated by comparing the numerical results with the testing ones. Such virtual tests provide a separated normal and shear behavior of honeycomb specimen, which allow for the determination of the yield envelope depicted in the macroscopic shear strength vs. compressive strength plane.

## 2. Numerical tests of honeycomb under combined shear-compression

Since the study is focused on the behavior of honeycomb under combined out-of-plane shear-compression, the modelling of the whole testing environment is not necessary. Thus, only the detailed honeycomb structure was modeled here and the loading environment was modeled by two rigid planes moving at the velocities measured during real tests. The commercial FE code of ABAQUS/explicit was employed for this numerical work.

### 2.1 Numerical specimen

The honeycomb structure studied here has the identical geometry to the hexagonal honeycomb used in the experiments presented in part I. It is composed of single-thickness walls (or thin walls) and double-thickness walls (or thick walls), having the following geometric parameters: single wall thickness h=76 μm, expansion angle α=30$^o$, and minimum cell diameter S=6.35 mm (as shown in Figure 1).

A complete model possesses the same size as the specimen employed in the experiments, which includes 39 cells on the honeycomb cross section. The dimensions of the specimen are 25×40×40 mm in the directions of T, L and W respectively (Figure 1).
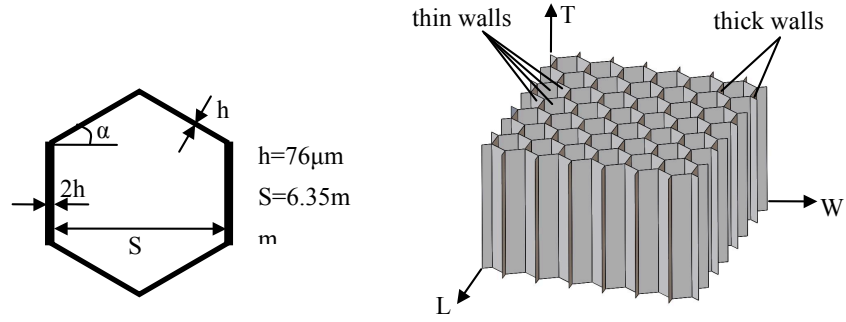
Figure 1 The geometry of a unit cell and the constructed honeycomb specimen

The thick walls in a real honeycomb are typically made of two single-thickness thin walls which are bonded together. In this model, we ignore the rare delamination of the bonded interfaces and consider the strength of the adhesive bond as infinite. Thus, the simulations are carried out for a monolithic honeycomb, where the thick walls are also represented by a single shell element layer but with a doubled thickness value.

The model is meshed with 4-node doubly curved thick shell elements with reduced integration, finite membrane strains, active hour-glass control and 5 integration points trough the cell wall thickness. In order to determine the appropriate element size, a convergence study was performed among element sizes of 1 mm, 0.5 mm, 0.25 mm and 0.125 mm. It seems that the results converge when the element size is equal to or below 0.25 mm. With selected element size of 0.25 mm, the complete-model has totally 232600 elements.

The numerical specimen is placed between two rigid planes moving with prescribed velocities that are defined with the real input and output velocities (denoted as $V_{input}$ and $V_{output}$ in Figure 2) measured during the combined shear-compression experiments (Part I of this study). In this model, general contact with frictionless tangential behavior is defined for the whole model excluding the contact pairs of rigid planes and tested honeycomb specimen, which are redefined by surface-to-surface rough contact to make sure that no slippage occurs.
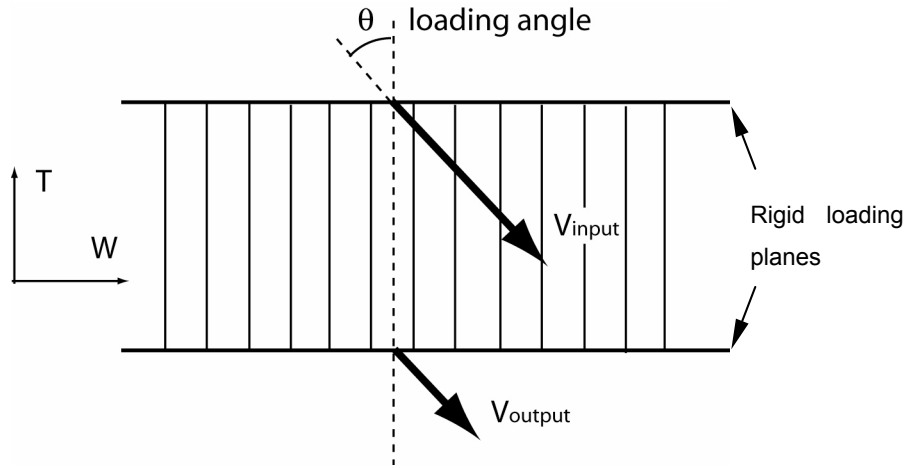
Figure 2 Scheme of loading velocities

As the real honeycomb is always far from perfect, it includes all kinds of imperfections which affect the initial peak value markedly, but have little influence to the crush behavior at large deformation period. These imperfections can be categorized into global ones and local ones, like irregular cell geometry, uneven or pre-buckled cell walls, wall thickness variation etc. Here in this work, we generated the imperfections by preloading the perfect specimen uniaxially by 0.1 mm before applying the prescribed experimental velocities. The value of 0.1 mm is chosen to make sure that the simulated initial peak is same as the one from experimental curve at uniaxial compression.

Quasi-static simulations were almost impossible to achieve with ABAQUS/Standard which uses Newton's method (or quasi Newton's method) as a numerical technique due to the complex nonlinear effects, e.g. the geometrical and material nonlinearity, the complex contact conditions as well as the local instability during crush. An alternative is to use also ABAQUS/Explicit for quasi-static problems. However, the explicit integration scheme of dynamic simulation codes usually leads to very small time step which in our simulation is around ten nanoseconds for the chosen element size. Thus, with the loading velocity of 0.1 mm/s, the computational duration for the quasi-static simulation (e.g. 180 s) will be too large. To overcome this difficulty, automatic mass scaling technique was employed to increase the time increment to 100 μs. The quasi-static loading conditions are guaranteed by ensuring

the ratio of the kinetic energy to the strain energy as a small value with the selected time increment.

A bilinear elasto-plastic material model was employed to describe the cell wall material of this aluminum honeycomb. The loading case of dynamic uniaxial compression is taken as calculating instance. The model parameters of base material such as yield stress and hardening modulus were determined by fitting the calculation result of uniaxial compression to the result from experiment (Table 1).

| Material | Density $\rho$ (kg/m$^3$) | Young's Modulus E (GPa) | Poission's Ratio $\nu$ | Yield Stress $\sigma_s$ (MPa) | Hardenning Modulus $E_t$ (MPa) |
|---|---|---|---|---|---|
| Aluminium | 2700 | 70 | 0.35 | 380 | 500 |

Table 1 Bilinear material parameters

Figure 3 shows the comparison between experimental and simulated pressure/crush curves, which validates the parameters of this bilinear material model.
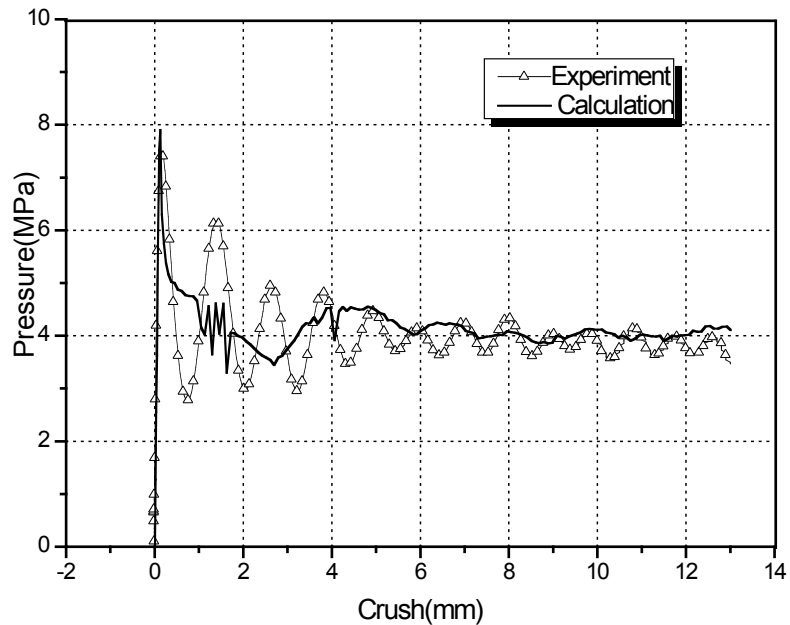


Figure 3 Comparison between numerical and experimental results

**2.2 Simplified models**

In order to reduce the calculation cost for this complete honeycomb model, numerical models with various simplifications can be also used. For example, some researchers [5,18] used one-dimensional beam elements with different microsections for the simulation of the in-plane behavior, while some others employed one layer of shell element according to the repeated behavior in cell axis direction [19]. As to the out-of-plane behavior, the honeycomb specimen was usually simplified into a unit cell or a row of cells because of its periodicity [9]. These simplifications may introduce some imprecisions to the numerical model. In order to check the potential errors, two simplified models were established. By comparing the results of these three models under uniaxial out-of-plane compression, the accuracy of the simplified numerical models were insured.

The so called row-model is made up of a row of cells based on the periodicity of honeycomb specimen in L direction (as shown in Figure 4) and will be used to investigate the combined shear-compression behavior of honeycomb in TW plane. The most simplified model consists of three conjoint half walls in "Y" configuration (denoted as cell-model as in Figure 4) and can be used only in uniaxial compression to make a comparison with the other two models. Both of the two simplified models have a length of 25 mm in T direction, and the same element size of 0.25 mm as in the complete model. The numbers of elements for row-model and cell-model are 28500 and 2100 respectively.
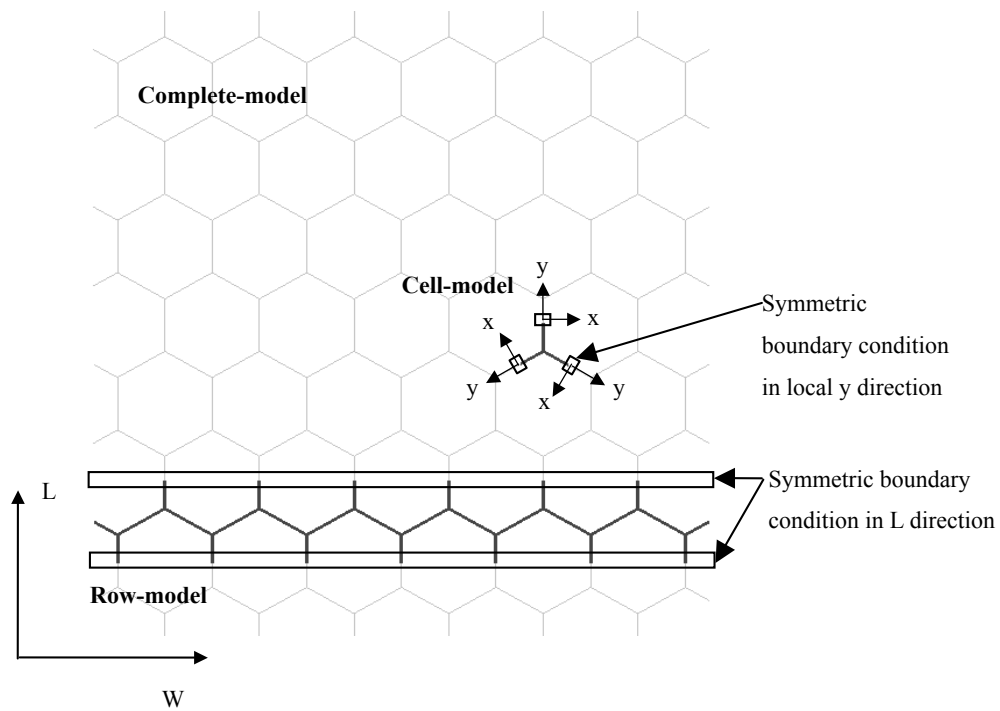
Figure 4 Scheme of complete and simplified models

The simplified models work with symmetric boundary conditions. These displacement constraints are applied to the row-model on the two boundaries in L-direction (as shown in Figure 4). For the cell-model, symmetric boundary conditions are performed on the three non-intersecting edges of each cell wall in local y-direction (as shown in Figure 4). The same method is employed to introduce imperfections into these simplified models.
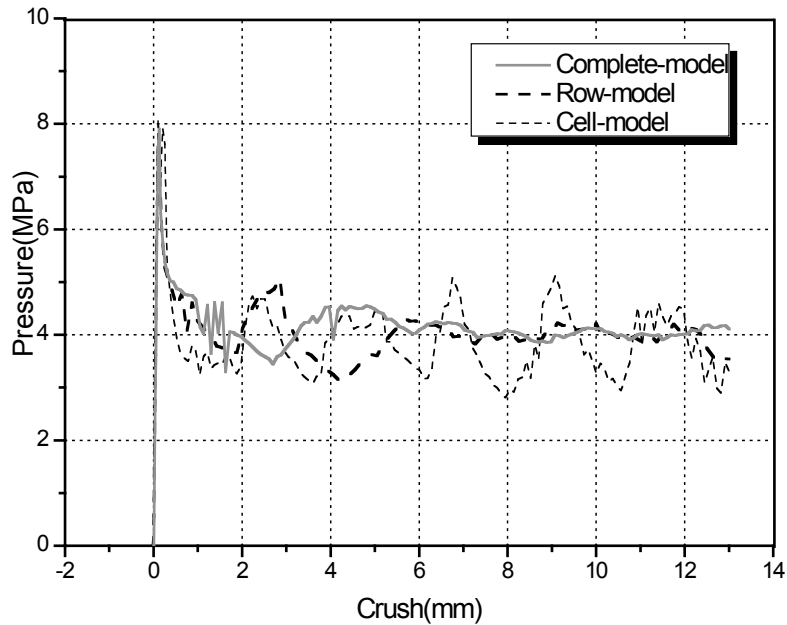
Figure 5 Comparison between the calculating results from three models

Figure 5 shows a comparison of pressure/crush curves for the three models. The row-model shows a good agreement with the complete-model while the cell-model exhibits significant fluctuations at the plateau stage which is probably due to the application of excessive symmetric boundary constraints. Actually, it is well known that the crushing behavior of honeycomb under out-of-plane compression is regulated by the progressive folding procedure of honeycomb cell walls. With the symmetric boundary conditions on three non-intersecting edges, the cell-model is actually equivalent to a honeycomb specimen consisting of repeated cells with identical deforming procedure, which results in strictly simultaneous collapse of honeycomb material in one folding layer. Thus, in the pressure/crush curve, each fluctuation represents one fold formation of the cell wall in honeycomb microstructure. While for the large size model, the neighboring cells interact with each other while forming the folds, and reach their local peak value successively, making the macroscopic resulting curves smoother.

As a conclusion, the cell model has some shortages in properly simulating the boundary condition and fails to calculate the honeycomb multiaxial behavior. Although an ideal model should be of the same dimension as the tested specimen, considering the contributions of

simplified models in reducing the time-expense of calculation, we finally chose the row-model for the subsequent calculations on the biaxial behavior of honeycomb under combined shear-compression.

# 3. Biaxial behavior of honeycomb under combined shear-compression

In this section, the results of four loading cases under combined out-of-plane shear-compression (in TW plane) with loading angles of $30^{o}$, $40^{o}$, $50^{o}$ and $60^{o}$ simulated with row-model for both dynamic and quasi-static cases are presented. We first carefully examined the validity of our numerical specimens by comparing the overall pressure/crush curves and the deforming mode with experimental results at various loading angles. Finally, the normal and shear behavior of numerical honeycomb under combined shear-compression could be separated.

## 3.1 Validation of numerical specimen

The overall pressure/crush curves are obtained from the calculated results in order to make a comparison between the experiments and the simulations. It is worth emphasizing that the variable "crush" is defined in Part I as the relative displacement component of the two moving bevels in $X_3$ direcion and the "pressure" as the $X_3$ force component divided by specimen cross-sectional area $S_s$. As a consequence, in the case of numerical combined shear-compression test, the pressure $P(t)$ is calculated by dividing the contact force component in the rigid planes moving direction ($X_3$ direction in Figure 6) with specimen area $S_s$. Its relationship with the directly obtained normal and shear contact forces is as follows:

$$P(t) = (F_n(t)\cos\theta + F(t)_s \sin\theta)/S_s \qquad (1),$$

where θ is the loading angle as defined in Part I. $F_n(t)$ and $F_s(t)$ are respectively the normal and shear contact forces at the interfaces of honeycomb specimen and rigid loading planes.
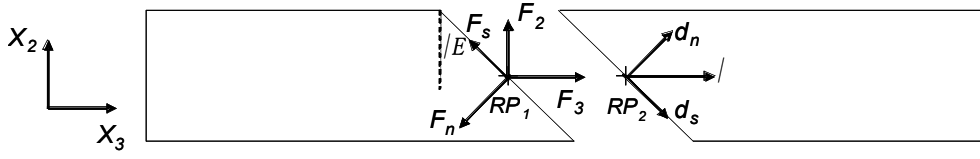
Figure 6 Scheme of the decompositions of force and crush

The overall crush $\Delta(t)$ is derived from the relative resultant displacement of the two reference points on rigid planes (Figure 6). It has a simple relationship with the normal and shear crush (denoted as $d_n(t)$ and $d_s(t)$), which is:

$$\Delta(t) = d_n(t)/\cos\theta = d_s(t)/\sin\theta \tag{2}$$

Figure 7 presents the experimental and calculated pressure/crush curves under dynamic uniaxial compression and combined shear-compression, for a representative loading angle $\theta=50^{\circ}$. Each curve has two distinct stages. During stage I (from the beginning of zero crush to the position of the initial peak), the slopes of elastic segment are in good agreement for the calculations and the experiments. In addition, with the employed magnitude of imperfection which is determined in complete-model under uniaxial compression, the initial peak of the calculated curve also agrees well with the experimental one for the displayed combined loading instance equally. During stage II (defined as the following crush period after stage I to 13 mm crush), the experimental curves have more fluctuations than the calculated ones, but still can be predicted in terms of average crush strength.

A comparison between the initial peak value as well as the average crush strength for every loading angle is described in Figure 8. The average crush strength is calculated by dividing the curve area of this plateau deforming region (absorbed energy) by the corresponding crush length (same formulas as used for experimental curves), which gives:

$$\bar{p} = \frac{1}{\delta_{\max} - \delta^*} \int_{\delta^*}^{\delta_{\max}} p\,d\delta \tag{3}$$

where $\delta^*$ denotes the crush value at the point of the initial peak for each of the overall pressure/crush curve. $\delta_{\max}$ is the maximum crush of the concerned crushing duration.

For the initial peak, a maximum difference of 4.9 % between the simulation and the experiment is found at loading angle of 50$^\circ$. For the average crush strength, the deviation is a little more significant at larger loading angles.
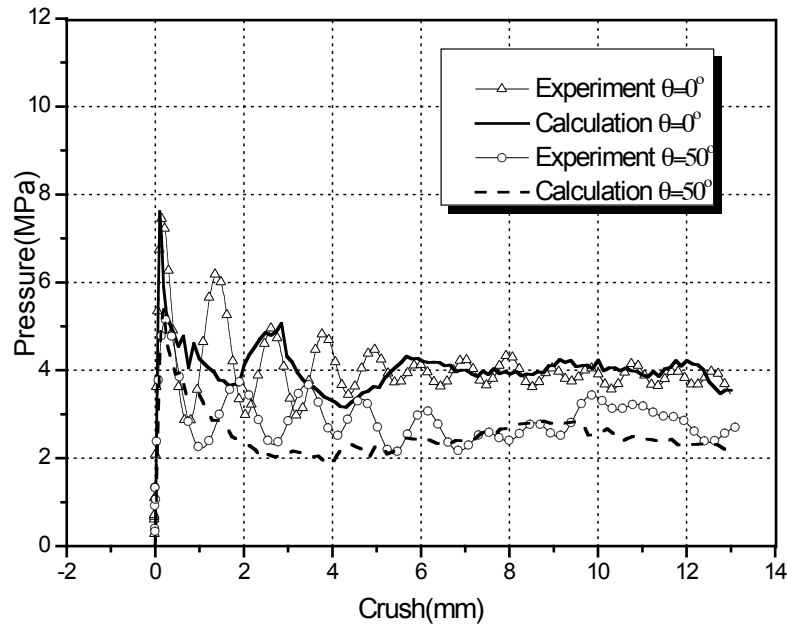


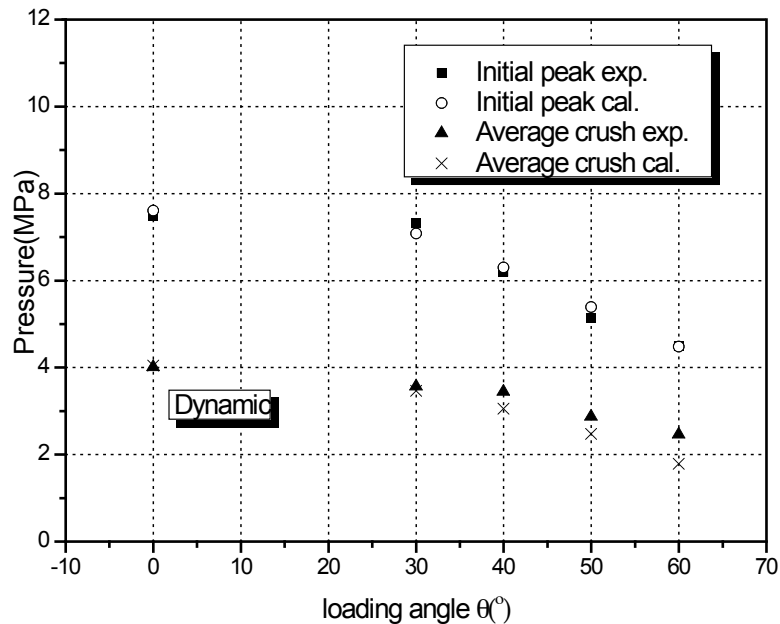Figure 7 Comparison of the dynamic pressure/crush curves from calculation and experiments



Figure 8 Comparison of the initial peak and average crush strength between dynamic calculations and experiments at various loading angles

The quasi-static virtual testing results for uniaxial compression and combined shear-compression at loading angle θ=50° are compared in Figure 9 together with the experimental curves. The numerical results show a good correlation with the experimental ones at the crushing stage II. The average crush strengths are calculated for all the loading angles and listed in Figure 10. The maximum error of 13.2 % is found at loading angle of 40°.
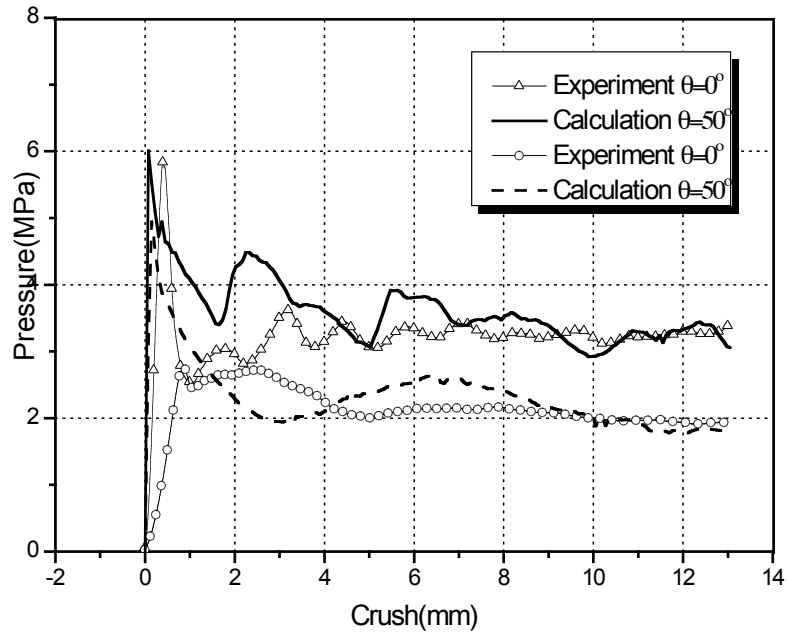


Figure 9 Comparison of the quasi-static pressure/crush curves from calculation and experiments
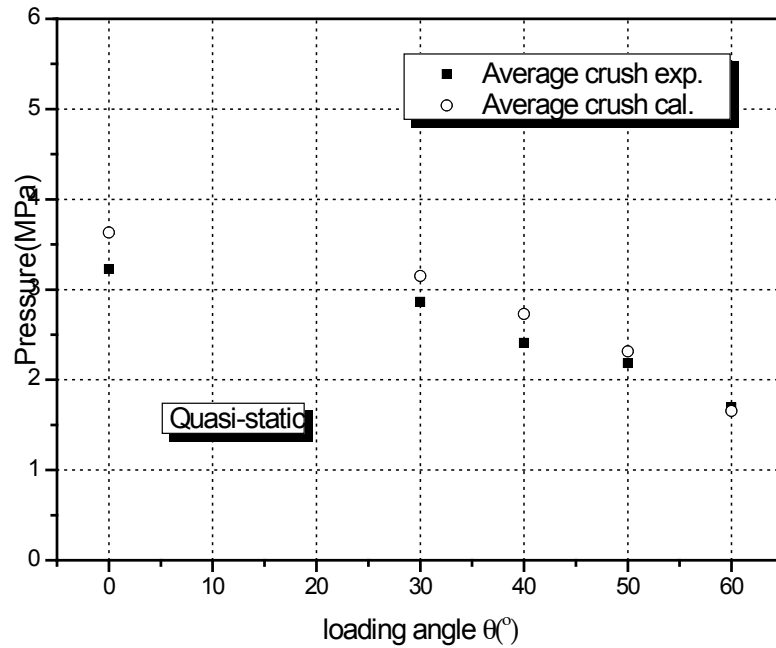
Figure 10 Comparison of average crush strength between quasi-static calculations and
experiments at various loading angles

Nevertheless, during stage I of the curves, a clear difference is found for both the ascending segment slope and the initial peak value that can be attributed to a slight slippage between specimen and bevels at the beginning of the experiment.

Furthermore, the simulated deforming pattern of honeycomb under combined shear-compression during stage II is also compared with the experimental results obtained with high speed camera. Figure 11 (a) and (b) show the specimens at dynamic loading of $\theta=30^{\circ}$ and at crush of 12 mm, and Figure 11 (c) and (d) for the quasi-static loading of $\theta=50^{\circ}$. It can be seen that the cell wall axis of all the specimens displayed incline during the crushing processes, and the inclined directions of the virtual and real specimens are in parallel to each other for the two loading angles. Besides, the phenomenon of two-side folding system is also found in the numerical results as discovered for most of the experimental shear-compression specimens.
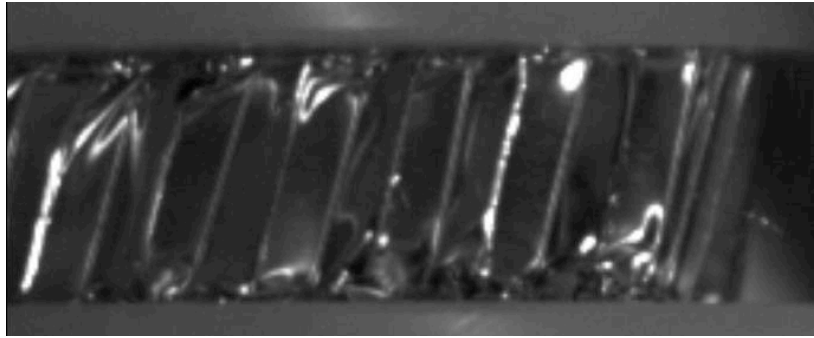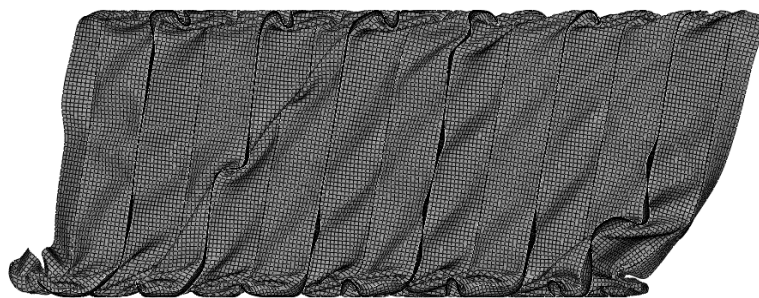
(a)
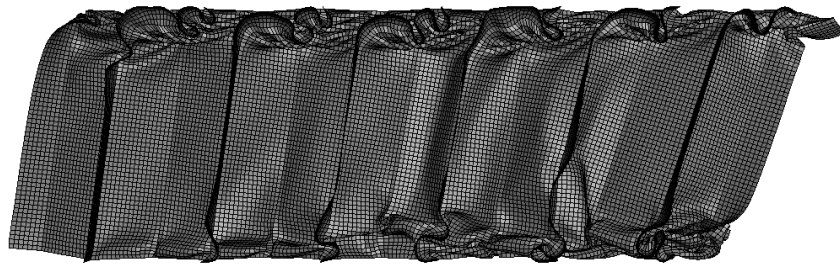


(b)
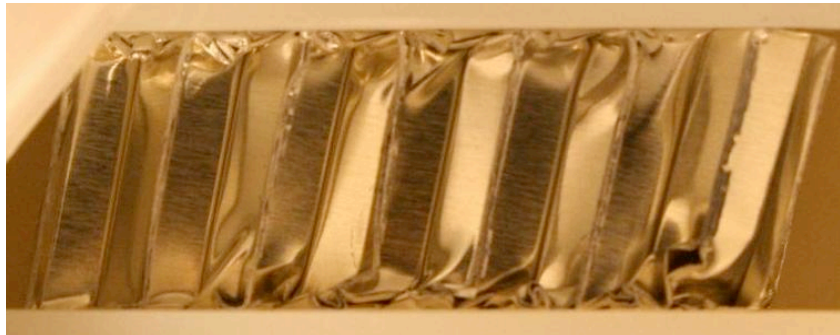


(c)



(d)

Figure 11 Comparison of deformation configuration of experimental ((a) and (c)) and calculating ((b) and (d))

honeycomb specimen under dynamic ($\theta=30^{o}$ (a) and (b)) and quasi-static ($\theta=50^{o}$ (c) and (d)) combined

However, the numerical result can not cover at the same time the two deforming modes (rotation of cell axis or not) found during experiments (Part I). Figure 12 illustrates the rotation angle α at 40 % mean compressive strain for every loading angle. It appears that our numerical specimen have a clear preference for the deforming mode with significant cell axis rotation.
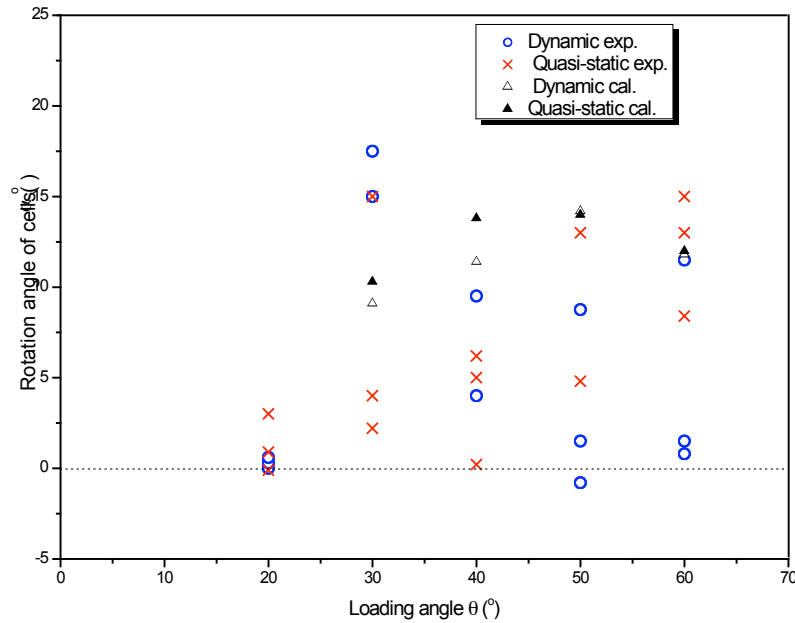


Figure 12 Comparison of the cell axis rotation at every loading angle from both experiments and simulations

## 3.2 Multiaxial behavior

The validation of the simulation work in section 3.1 shows that the virtual testing results can represent well the experimental ones with the exception of quasi-static initial peak forces. These virtual combined shear-compression tests provide more information than the real experiments and enable us to study the normal and shear behavior of honeycomb separately.
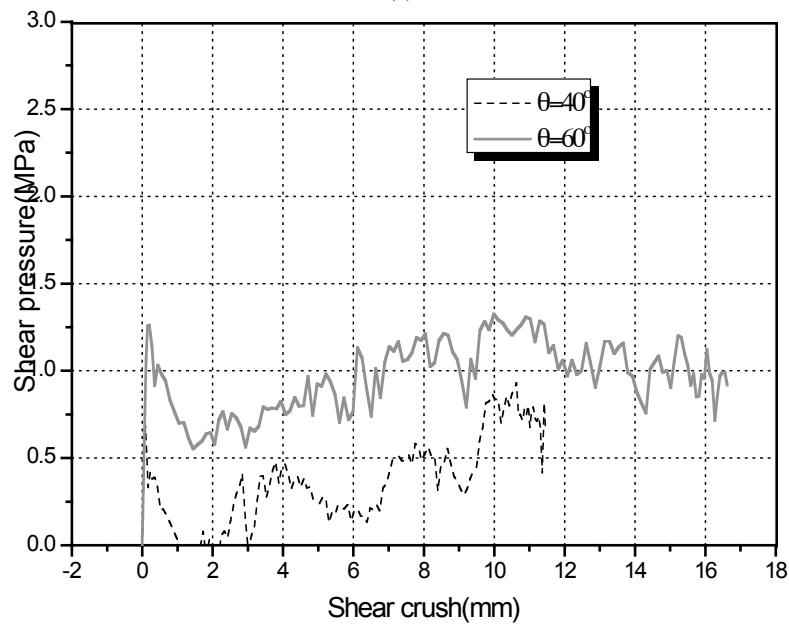
The separated normal and shear pressure/crush curves under dynamic loading are shown in Figure 13 (a) and (b) respectively. It is noted that the normal and shear pressures are calculated from the normal and shear contact forces ($F_n(t)$ and $F_s(t)$) at the interfaces between rigid loading planes and honeycomb specimen. For the sake of clarity, only 0° (not included in shear behavior), 40° and 60° are displayed.

It is observed in Figure 13(a) that the level of normal pressure/crush curves decreases when the loading angle increases. The shear behavior is generally weaker than the normal one (as shown in Figure 13 (b)) and the initial peak becomes inconspicuous with respect to the succeeding plateau. The strength level of the shear curves at the plateau stage increases with increasing loading angle, which has the opposite trend with normal behavior.

It is worthwhile to recall that, in the experimental tests, the change of the loading angle modifies not only the ratio between normal and shear loadings but also the measured axis-force component. Here in this numerical test, such an ambiguity is eliminated because we measured directly the normal and shear strength. The results shown in Figure 13 do mean a lower resistance of honeycomb structure to compression under an increasing additional shear.
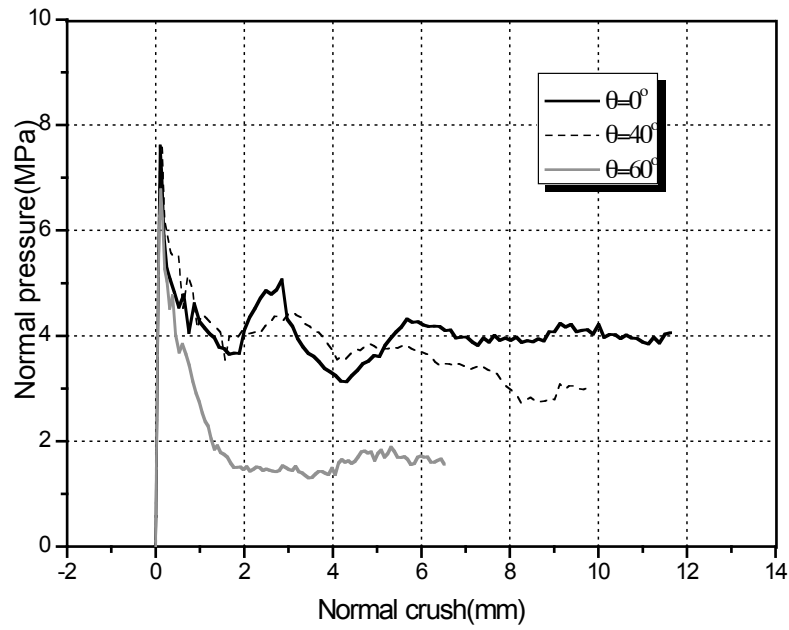
(a)



(b)

Figure 13 Normal and shear behaviors of honeycomb under dynamic combined

Under quasi-static loading, the normal and shear pressure crush curves show a great similarity to the dynamic ones, i.e. the normal strength decreases with the loading angle whereas the shear strength increases. Moreover, a comparison between the quasi-static and the dynamic curves shows that the loading rate will also affect the normal and shear behavior of honeycomb under combined shear-compression. Figure 14 displays the dynamic and

quasi-static normal and shear curves at θ=40°. An obvious enhancement is found for both of the two groups of curves.
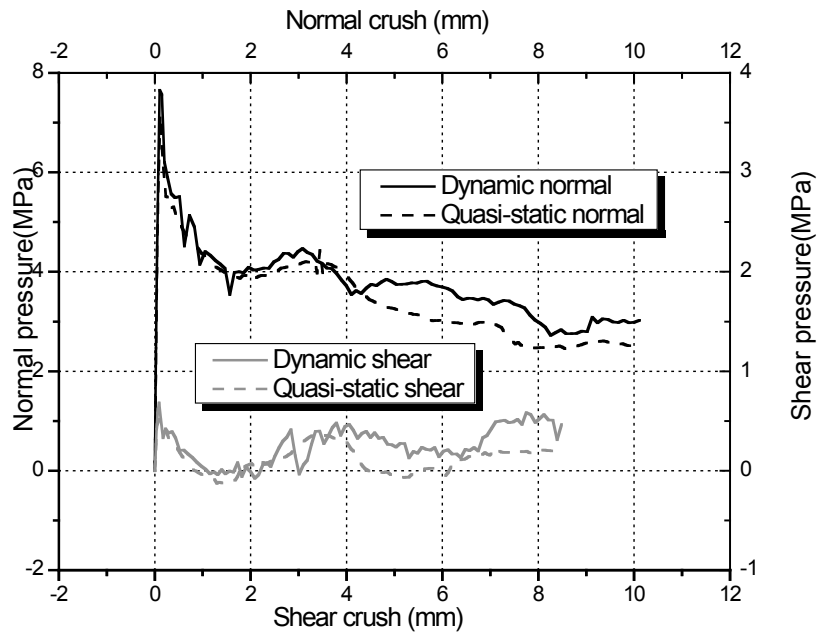


Figure 14 Comparison between dynamic and quasi-static normal and shear pressure/crush curves

at loading angle of 40°

The average crush strength of normal and shear behavior were calculated for both dynamic and quasi-static loading at every loading angle as done in section 3.1 for the overall pressure/crush curves. All these average values are collected in Figure 15, which shows clearly the change of the normal and shear crush strength along with the loading angle as well as a strength enhancement under impact loading for every loading angle.
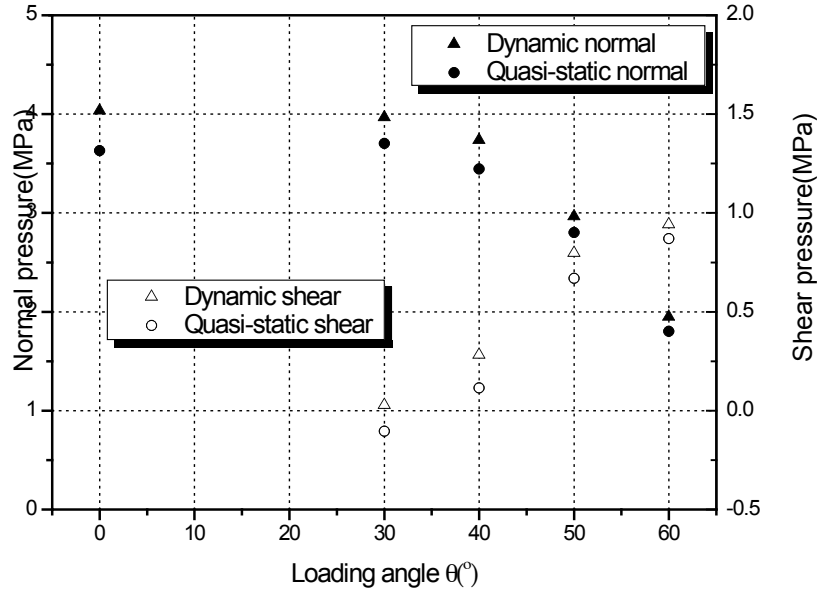
Figure 15 Comparison between dynamic and quasi-static normal and shear pressure vs. loading

## 3.3 Macroscopic yield envelop estimation

Figure 16 shows the distribution of calculated honeycomb biaxial behavior on the normal average strength vs. shear average strength plane during the stage II. An elliptical shape is found for both the quasi-static and dynamic loading cases (Eq. 4).

$$\left(\frac{\sigma}{\sigma_0}\right)^2 + \left(\frac{\tau}{\tau_0}\right)^2 = 1, \tag{4}$$

where $\sigma_0$ and $\tau_0$ are respectively the normal crushing strength under uniaxial compression and the shear crushing strength under pure shear loading. By fitting the data with Levenberg-Marquardt algorithm (LMA), these two parameters are identified to be 3.98 MPa and 1.11 MPa under dynamic loading and 3.57 MPa and 1.02 MPa under quasi-static loading.

It is found in Figure 16 that the expansion of the crush envelope from quasi-static to dynamic loading is almost isotropic, even though the normal strength/shear strength ratio for one same loading angle is different under quasi-static and dynamic loading. It means that the dynamic biaxial strength for this honeycomb might be derived by using the enhancing ratio of uniaxial compression and the quasi-static crush envelope.
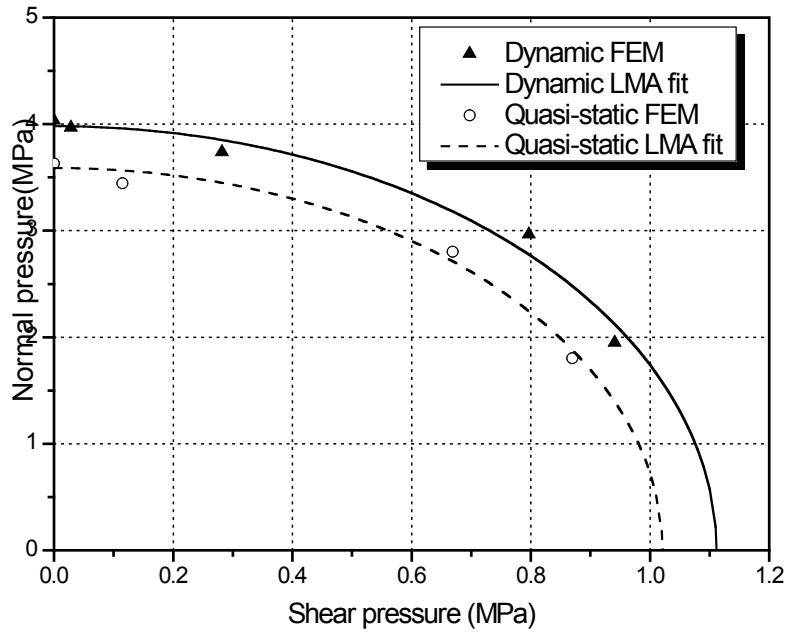
Figure 16 Crushing envelopes in normal strength vs. shear strength plane

## 4. Conclusions

This study proposed a new method of investigation of the dynamic biaxial behavior of honeycomb by combining the experiments based on SHPB technique and the FEM simulations.

A numerical specimen was built with simplified row model and identified material parameters and it provided simulated results in good agreement with the experiments in terms of deforming mode and the overall pressure/crush curves which were the final obtained information from the new designed combined shear-compression loading experiments.

Such numerical virtual tests enabled to separate the normal and shear behavior of honeycomb. It showed that the strength of honeycomb under compression is largely affected by the additional shear loading and exhibits a significant decrease while increasing shear loading. An obvious enhancement was also observed at dynamic loading for both the normal and shear behavior with respect to the quasi-static case at every loading angle.

In order to describe the dynamic and quasi-static biaxial behavior of honeycomb at macroscopic level, an elliptical criterion in the plane of normal strength vs. shear strength can be derived with a set of parameters obtained by fitting the data with Levenberg-Marquardt

algorithm. The expansion of the crush envelope with the loading rate happened to be isotropic for the studied honeycomb in combined out-of-plane shear-compression in T and W direction.

## Acknowledgement

## Reference

[1]. L. J. Gibson, M. F. Ashby, Cellular material: structure and properties, 2nd Ed., Cambridge University Press, Cambridge, UK. (1997)

[2]. L. J. Gibson, M. F. Ashby, J. Zhang, T.C.Triantafillou, Failure surfaces for cellular material under multiaxial loads-I. modeling. Int. J. Mech. Sci. 31, 635-663 (1989)

[3]. J. W. Klintworth, W. J. Stronge, Elasto-plastic yield limits and deformation laws for transversly crushed honeycombs. Int. J. Mech. Sci. 30, 273-292 (1988)

[4]. M. Y. Yang, J. S. Huang, Elastic buckling of regular hexagonal honeycombs with plateau borders under biaxial compression. Compo. Struct. 71 229-237 (2005)

[5]. S. D. Papka, S. Kyriakides, In-plane biaxial crushing of honeycombs-Part II: Analysis. Int. J. Solids Struct. 36 4397-4423 (1999)

[6]. M. Doyoyo, D. Mohr, Microstructural response of aluminum honeycomb to combined out-of-plane loading. Mech. Mater. 35 865-876 (2003)

[7]. D. Mohr, M. Doyoyo, Experimental investigation on the plasticity of hexagonal alumininum honeycomb under multiaxial loading. J. Appl. Mech. 71 375-385 (2004)

[8]. S.T. Hong, J. Pan, T. Tyan, P. Prasad, Quasi-static crush behavior of aluminum honeycomb specimens under compression dominant combined loads. Int. J. Plasticity 22 73-109 (2006)

[9]. D. Mohr, M. Doyoyo, Deformation-induced folding systems in thin-walled monolithic hexagonal metallic honeycomb. Int. J. Solids and Struct. 41 3353-3377 (2004)

[10]. D. Mohr, M. Doyoyo, Large plastic deformation of metallic honeycomb: Orthotropic rate-independent constitutive model. Int. J. Solids and Struct. 41 4435-4456 (2004)

[11]. E. Wu, W.S.Jiang, axial crush of metallic honeycombs, Int. J. Impact Eng. 19 439-456 (1997).

[12]. W. E. Baker, T. C. Togami, J.C.Weydert, static and dynamic properties of high-density metal honeycombs. Int. J. Impact Eng. 21 149-163 (1998).

[13]. H. Zhao, S. Abdennadher, On the strength enhancement of rate insensitive square tubes under impact loading, Int. J. Solids Struct. 41 6677-6697 (2004).

[14]. J. J. Harrigan, S. R. Reid, C. Peng, Inertia effects in impact energy absorbing materials and structures. Int. J. Impact Eng. 22 955-979 (1999).

[15]. I. Elnasri, S. Pattofatto, H. Zhao, H. Tsitsiris, F. Hild, Y. Girard, Shock enhancement of cellular structures under impact loading: Part I Experiments, J. Mech. Phys. Solids, 55 2652–2671 (2007).

[16]. S.T. Hong, J. Pan, T. Tyan, P. Prasad. Dynamic crush behaviors of aluminum honeycombs specimens under compression dominant inclined loads. Int. J. Plasticity, 24 89-117 (2008).

[17]. J. Chung, A. M. Waas. Compressive response of circular cell polycarbonate honeycombs under inplane biaxial static and dynamic loading. Part I:experiments. Int. J. Impact Eng. 27 729-754 (2002).

[18]. A. Hönig, W. J. Stronge, In-plane dynamic crushing of honeycombs. Part I: crush band initiation and wave trapping. Int. J. Mech. Sci. 44 1665-1696 (2002).

[19]. Z. Zou, S. R. Reid, P. J. Tan, S. Li, J. J. Harrigan, Dynamic crushing of honeycombs and features of shock fronts. Int. J. Impact Eng. 36 165-176 (2009).